Gut microbial interaction networks control autoimmunity to neuroretina

Amy Zhang[1#], Reiko Horai[1#*], Yingyos Jittayasothorn[1], Jonathan H. Badger[2], Zhichao Wu[3], Akriti Gupta[1], Samyuktha Arunkumar[1], Caitlin E. Murphy[1], Guangpu Shi[1], Vijayaraj Nagarajan[1], John A. McCulloch[2], Shilpa Kodati[1], H Nida Sen[1], Jung Wha Lee[1], Jonathan P. Jacobs[4], Xiaoyan Xu[1], Mary J. Mattapallil[1], Zixuan Peng[1], Biying Xu[1], Robert J. Palmer[5], Nadim Majdalani[6], Kenya Honda[7], Colm O'hUigin[2], Rachel R. Caspi[1*]

[1]Laboratory of Immunology, National Eye Institute, National Institutes of Health, Bethesda, MD, USA

[2]Genetics and Microbiome Core, Laboratory of Integrative Cancer Immunology, Center for Cancer Research, National Cancer Institute, National Institutes of Health, Bethesda, MD, USA

[3]Laboratory of Pathology, Center for Cancer Research, National Cancer Institute, National Institutes of Health, Bethesda, MD, USA

[4]Goodman-Luskin Microbiome Center, David Geffen School of Medicine at UCLA, Los Angeles, CA, USA

[5]Structural Biochemistry Unit, National Institute of Dental and Craniofacial Research, National Institutes of Health, Bethesda, MD, USA

[6]Laboratory of Molecular Biology, Center for Cancer Research, National Cancer Institute, National Institutes of Health, Bethesda, MD, USA

[7]Keio University School of Medicine, Tokyo, Japan

[#]Equal contribution

*Correspondence to:

Rachel R. Caspi (caspir@nei.nih.gov)

Laboratory of Immunology, National Eye Institute, National Institutes of Health
10 Center Drive, 10/10N248, Bethesda, MD 20892-1857, USA

Reiko Horai (hreiko@nih.gov)

Laboratory of Immunology, National Eye Institute, National Institutes of Health
10 Center Drive, 10/10S243, Bethesda, MD 20892-1857, USA

Funding: NIH/NEI Intramural funding, Project Number EY000184

Commercial Disclosures: None

Running title: Gut microbial interactions drive autoimmune uveitis

KEYWORDS

autoimmune uveitis, T cell receptor transgenic mice, humanized gnotobiotics, fecal microbiota reconstitution, microbial interaction, short chain fatty acids

ABSTRACT

The gut microbiome influences the development of immune-mediated inflammatory diseases. One such condition is autoimmune uveitis, a sight-threatening ocular inflammation driven by retina-specific T cells[1]. Using a model of spontaneous experimental autoimmune uveitis (sEAU) we showed that gut commensals provide immune stimuli that trigger the disease[2]. Here we report that uveitis-promoting microbes are present in human gut flora and that colonization of germ-free (GF) mice with commensal flora from healthy human donors was sufficient to provoke disease. Severity of sEAU correlated with expansion of Akkermansia and contraction of short-chain fatty acid (SCFA)–producing Firmicutes, followed by decreased SCFA levels and a dominant gut Th1 effector response. Mechanistic gain-of-function experiments, enriching GF sEAU mice with Akkermansia, reproduced these microbiome, metabolite and immune phenotype shifts, and exacerbated disease. We propose that Akkermansia promotes autoimmunity by outcompeting SCFA-producers and enhancing Th1-type responses. Notably, an inverse correlation between Akkermansia (Verrucomicrobia) and Firmicutes was also present in fecal microbiome of patients with uveitis, multiple sclerosis and Crohn's disease. These findings reveal a stereotypic gut microbial interaction network that regulates systemic immune balance, and may represent an ecologically conserved mechanism through which the gut microbiome modulates autoimmune and inflammatory diseases.

INTRODUCTION

Immune-privileged tissues are increasingly recognized as sites where host–microbiota interactions influence immunological balance in autoimmune and inflammatory diseases[3,4]. Multiple mechanisms have been proposed that explain the central role of microbiota in driving inflammation in the central nervous system (CNS), including innate and adaptive effects such as molecular mimicry[2,5], bystander activation[6], epitope spreading[7,8] and dual T cell receptors (TCRs)[9]. The eye, especially the neuroretina, is part of the CNS and represents a quintessential immune-privileged tissue, making it a valuable model to study immune privilege and autoimmunity in the CNS.

Autoimmune uveitis is a T cell-driven intraocular inflammation of unknown etiology that targets the neuroretina and can lead to blindness[1]. It is represented by the models of experimental autoimmune uveitis (EAU) in animals. EAU is induced in wild type mice by immunization with the retinal antigen IRBP[1], or can develop spontaneously (sEAU) in mice expressing a transgenic IRBP-specific TCR cloned from the immunization induced model (line R161H)[10]. Our previous studies highlighted the critical role of gut microbiome in triggering sEAU by providing antigenic stimuli that activate retina-specific T cells[2]. Subsequent research reported inhibitory effects of microbiome depletion also in induced EAU[11], where the antigen is provided, emphasizing the antigen-independent (innate?) effects of gut microbes on EAU. Interestingly, gut microbiome studies in uveitis patients have revealed differences in gut flora between patients and healthy controls[12-16], but mechanistic information could not be resolved.

Because inductive events and causal relationships cannot be studied in patients, we employed the model of sEAU in R161H TCR transgenic mice[10], which may provide a more physiological system to study triggers delivered by the microbiota. To gain mechanistic insights into how human gut microbiota might affect the development of autoimmune uveitis, we created gnotobiotic breeding colonies of R161H mice harboring healthy human gut flora by reconstituting GF parental mice with fecal material from three healthy human donors. The rationale for focusing on healthy donors is that *(i)* every uveitis patient was once a healthy person, so by definition, uveitis-relevant microbes should be present in the healthy person's gut flora, and *(ii)* the composition of patient

31 flora could have been altered by their disease or by their treatment, confounding data
32 interpretation.

33 Using a multiomic strategy that integrates microbial, metabolomic and immune profiling of
34 human flora (HuFl)-reconstituted R161H mice, combined with analyses of human
35 autoimmune disease datasets, we identified a microbial interaction network comprising
36 an "Akkermansia/Verrucomicrobia—Firmicutes axis" that appears to regulate
37 autoimmunity. Our data points to an underexplored but fundamental mechanism, where
38 interactive relationships in the microbial community play a central role in regulation of
39 autoimmune disease pathogenesis by microbiota[17].

40 **RESULTS**

41 **1. Human gut commensals support development of spontaneous experimental**
42 **autoimmune uveitis (sEAU)**

43 R161H mice harboring mouse microbiota (specific-pathogen-free, SPF) typically develop
44 moderate to severe uveitis with high penetrance (100% incidence by two months of
45 age)[10]. To first assess whether human gut microbiota affect uveitis development, we
46 developed "humanized gnotobiotic" R161H mouse lines as our pre-clinical model, by
47 reconstituting breeding pairs of GF R161H mice with gut microbiota from three healthy
48 human subjects—U, V, and W. Each line was maintained in separate isolators through
49 successive generations, so that the offspring acquired the human flora naturally from
50 their respective parents (Fig. 1a).

51 Microbiome sequencing results showed successful engraftment of human flora in
52 gnotobiotic R161H mice. The succession of gut microbiota through generations of
53 breeding in gnotobiotic isolators did not appear to diminish the differences between
54 individual cohorts, and each U, V, or W mouse recipient cohort preserved the microbial
55 signatures of its original donor (Fig. 1b).

56 Human commensal microbes supported uveitis development in R161H mice. Although
57 HuFl mice display a broad spectrum of disease scores, the scores were on average lower

58 than those of SPF mice that harbor normal mouse flora (Fig. 1c & Extended Data Fig.
59 1a). We did not observe obvious sex differences with respect to disease severity in HuFI
60 mice (Extended Data Fig. 1b). Immune phenotype of colonic $CD4^+$ T cells, based on a
61 range of cell surface and intracellular markers, clearly distinguished HuFI mice from GF
62 and SPF mice (Fig 1d & Extended Data Fig. 1c-e). The HuFI mice showed a spectrum of
63 disease scores and memory marker expression between GF (low) and SPF (high) mice
64 (Fig. 1e), had fewer IFN-γ-producing Th1 and IL-17A-producing Th17 effector cells and
65 more regulatory T cells (Tregs) expressing Foxp3 and IL-10 than did SPF mice (Fig. 1f-
66 g). This immune phenotype was consistent with other activation markers and Th1/Th17
67 signature molecules (Extended Data Fig. 1e). This phenotype may explain the lower
68 disease scores that they developed.

69 **2. HuFI sEAU tracks with a dominant Th1 phenotype and abundance of**
70 **Verrucomicrobia/Akkermansia**

71 Since both Th1 and Th17 effector phenotypes can drive autoimmune uveitis[18-20], we set
72 out to define the immune signatures that associate with disease in the HuFI model. We
73 categorized histological scores into high (score ≥ 1.5), mid (0.75 < score < 1.5), and low
74 (score ≤ 0.75) to facilitate statistical analysis. Interestingly, IFN-γ-producing CD4 T cells,
75 rather than IL-17A producers, in the gut (and other tissues) associated strongly with
76 severe disease phenotype (Fig. 2a-d). This suggests that uveitis development in HuFI
77 mice is more dependent on Th1 than Th17.

78 Microbiome analysis of parental and offspring HuFI mice showed that colonized mice
79 adopted only a subset of the original donor taxa (Extended Data Fig. 2a-b). This could be
80 a result from loss during human stool sample preservation and transfer processes, and/or
81 from inefficient engraftment of some non-native microbes to the gut environment of a
82 different host species. However, in terms of the overall microbial composition, each
83 mouse cohort remained closer to their original donor, preserving a distinct microbial
84 footprint (Fig. 1b & Extended Data Fig. 2c-d). Differences between female *vs.* male HuFI
85 mice in terms of microbial abundance and composition were minimal, if any, compared to
86 the differences based on human donors (Extended Data Fig. 2e-f). This is compatible

with the apparent lack of sex differences in disease severity of HuFI mice (Extended Data Fig. 1b).

We then explored how gut microbiome associates with severity of uveitis. Correlational heat map of major bacterial taxa at the family level revealed strong links between several taxa and histology scores (Fig. 2e). Among them, Akkermansia (the only representative of Verrucomicrobia in HuFI mice) correlated with high disease scores (Pearson r = 0.5, FDR <0.05), whereas certain members of the Firmicutes phylum were correlated with low disease scores (Pearson r = -0.3, FDR <0.05). Differential abundance analysis between high and low histology categories consistently showed that Akkermansia was enriched in mice with high disease, whereas Firmicutes (especially Clostridia) were enriched in mice with low disease (Fig. 2f-g & Extended Data Fig. 2g).

3. SCFA signatures are enriched in low disease HuFI mice or healthy subjects

SCFAs are metabolites of commensal gut microbes resulting from fermentation of dietary fiber, and have anti-inflammatory properties in a range of pathological conditions[21]. Some SCFAs, e.g. butyrate and propionate, may have therapeutic potential in induced EAU[22,23]. In the current study, a key observation from differential abundance analyses of mice with low and high disease scores was that SCFA-producing Firmicutes were associated with lower sEAU scores (Fig. 2e). Therefore, it appeared plausible that SCFAs may also have the potential to modulate sEAU.

To address this, we mined functional gene signatures from shotgun metagenomic sequences of HuFI mice. Genes known to be involved in SCFAs synthesis and metabolism were mapped to the simplified pathways shown in Fig. 3a. Consistent with the observed differences in microbial abundance (Fig. 2e), the genes involved in main SCFA pathways were enriched in mice with low disease scores and reduced in mice with high disease scores (Fig. 3b). In agreement with the pathway analysis, metabolomic quantification of SCFAs in the gut and serum of the mice confirmed that higher disease scores were associated with lower SCFA concentrations both locally and systemically (Fig. 3c).

115 We next examined whether this signature was present in a cohort of uveitis patients seen
116 at the NEI clinic, compared to healthy controls. Because uveitis is a heterogenous
117 disease, we focused on a subset of patients whose disease was restricted to the eye
118 (idiopathic uveitis, Vogt-Koyanagi-Harada disease/sympathetic ophthalmia and birdshot
119 chorioretinopathy), as modeled by EAU, rather than being part of a systemic syndrome.
120 Similarly to the HuFI R161H mice, enzymes involved in acetate, butyrate and propionate
121 pathways (Fig. 3d) and their corresponding SCFAs (Fig. 3e), were reduced in uveitis
122 patients compared to healthy controls. This supports a role for SCFAs in regulation of
123 human uveitis.

124 **4. Akkermansia negatively correlates with Firmicutes in both sEAU and clinical**
125 **uveitis**

126 Among all taxa in HuFI mice, Akkermansia abundance was shown to be a prominent
127 correlate of severe uveitis and IFN-γ-producing CD4+ T cells in the gut (Fig. 2e-f,
128 Extended Data Fig. 3a–b), whereas SCFA-producing Firmicutes were reduced in the
129 same animals (Fig. 2e, g). We therefore analyzed their relative abundance and potential
130 interdependence to determine whether competitive interactions between these taxa might
131 contribute to autoimmune uveitis.

132 We first quantified abundance of Akkermansia and Firmicutes, and found them to be
133 inversely correlated (Fig. 4a). An in-depth computational analysis of the bacterial
134 association network confirmed the negative correlation between Akkermansia and
135 multiple families of SCFA-producing Firmicutes (Fig. 4b, Extended Data Fig. 3c). Levels
136 of major SCFAs in feces also exhibited an inverse correlation with Akkermansia
137 abundance (Fig. 4c). Taken together, this supports an interpretation of a negative
138 interaction between Akkermansia and a range of SCFA-producing microbes.

139 Similarly, gut microbiome interaction networks of uveitis patients displayed a negative
140 relationship between Verrucomicrobia (primarily Akkermansia) and SCFA-producing
141 Firmicutes (Clostridia, class level), but this relationship was not evident in healthy
142 subjects (Fig. 4d). This supports the relevance of the sEAU model to clinical disease.

143 **5. Akkermansia promotes uveitis by outcompeting SCFA producers and**
144 **decreasing circulating SCFA levels**

145 To validate the proposed microbiome interaction network *in vivo*, we used a gain-of-
146 function approach, where GF R161H mice received Akkermansia alone or Akkermansia
147 mixed with HuFI mouse donor fecal flora. In the first paradigm, we associated GF mice *de*
148 *novo* with cultured *Akkermansia muciniphila* (the type species of Akkermansia) or with
149 sterile PBS as control, and maintained them in static microisolators using sterile handling
150 techniques, to minimize additional microbial exposure (Extended Data Fig. 4a). This
151 approach resulted in a minimal gut microbial population of very low diversity (≤10 total
152 detectable taxa/mouse), dominated by Verrucomicrobia (Akkermansia) and Firmicutes
153 (Extended Data Fig. 4b-d).

154 First paradigm: A single oral gavage led to successful and sustained engraftment of
155 Akkermansia, and resulted in higher uveitis scores (Extended Data Fig. 4e-f). Akkermansia
156 was nearly undetectable in the PBS control group, whose gut microbiota became
157 dominated by Firmicutes (Extended Data Fig. 4g). As such, the relative abundances of
158 Akkermansia and Firmicutes showed a near-perfect inverse relationship (r-squared > 0.99,
159 $p < 0.0001$) (Extended Data Fig. 4h). Other bacterial phyla that are prominent in normal
160 mouse or human gut flora were low or on the borderline of detectability (Extended Data
161 Fig. 4i). Thus, this model reflects a minimal-diversity gut ecosystem dominated by the two
162 taxa that we hypothesize to display competitive dynamics that control expression of
163 disease.

164 Second paradigm: To examine this hypothesis under more physiological conditions, where
165 Akkermansia is not given a major “head start”, we associated GF R161H mice with flora
166 from HuFI mice (selected for low disease and low abundance of Akkermansia) “spiked”, or
167 not, with cultured *A. muciniphila* (Fig. 5a). Fecal microbiome profiling confirmed successful
168 microbial engraftment and stability of Akkermansia-high or Akk-low status (Fig. 5d &
169 Extended Data Fig. 5a). Akkermansia “spiked” flora induced more severe uveitis than base
170 HuFI alone (Fig. 5b-c) and the relative abundances of Akkermansia and Firmicutes were
171 consistently inversely correlated (Fig. 5e). Notably, among the major bacterial phyla,

172 Firmicutes was the only phylum whose abundance was decreased in Akk-enriched mice
173 (Fig. 5d & Extended Data Fig. 5b), particularly those taxa considered "professional" SCFA
174 producers[24] (Extended Data Fig. 5c). To confirm that the effects described above were
175 indeed Akkermansia-specific, we associated GF R161H mice with the same HuFl "spiked"
176 with *E. coli*. The disease-promoting phenotype and the reduction in Firmicutes abundance
177 were not recapitulated, supporting the notion that the observed effects were specific to
178 Akkermansia (Extended Data Fig. 5d-f). Together, these results reinforce a dynamic
179 balance between Akkermansia and Firmicutes that modulates autoimmune uveitis in a
180 physiologically relevant setting.

181 To mechanistically link Akkermansia–Firmicutes dynamics with circulating SCFA levels
182 available to regulate uveitis-relevant immune responses, we measured serum SCFAs and
183 host immune parameters. All three major SCFAs – acetic, butyric and propionic acids –
184 were reduced in Akk-high mice compared with Akk-low mice (Fig. 5f), consistent with the
185 negative relationship between Akkermansia and Firmicutes. This reduction was not
186 observed in the *E.coli* control group (Extended Data Fig. 5g). Given the known
187 immunomodulatory role of SCFAs[21] , we examined whether this metabolomic shift was
188 associated with an altered systemic effector response. In both the Akk-associated minimal
189 flora model and the Akk-enriched HuFl model, reduced serum SCFAs were tightly coupled
190 with elevated serum and/or gut IFN-γ responses (Fig. 5g–j). These results implicate that
191 SCFAs may regulate disease by dampening the Th1 effector response.

192 The final mechanistic question was whether Akkermansia can provide surrogate antigenic
193 stimuli to trigger activation of the R161H TCR-expressing cells in the gut[2]. To address this,
194 we used an *in vitro* activation assay, where naïve R161H CD4 T cells and antigen-
195 presenting cells were cultured with Akk-rich HuFl gut content extracts, or with heat-killed
196 Akkermansia. Unlike SPF gut flora extracts or the cognate peptide antigen[2,10], neither
197 Akkermansia preparation activated the retina-specific T cells, as measured by expression
198 of CD69 and Nur77 (Extended Data Fig. 6a-b), indicating that Akkermansia was not acting
199 as an antigen mimic.

200 Single cell RNA-seq analysis of colonic CD4 T cells, of which an average of 15%
201 expressed the R161H TCR, revealed that both R161H TCR-expressing and non-R161H
202 (endogenous) T cells had a Th1, rather than a Th17, signature, that positively correlated
203 with abundance of Akkermansia (Extended Data Fig. 6c-d). Thus, Akkermansia appears
204 to skew the T cell response phenotype independently of the T cell antigen specificity,
205 which for non-R161H cells could be other gut microbes or food antigens. VDJ analysis
206 did not reveal evidence for a 2nd TCR among R161H TCR+ cells. In addition, *in silico*
207 analysis did not reveal shared sequence(s) between Akkermansia and IRBP$_{161\text{-}180}$, which
208 is the cognate R161H TCR epitope. We interpret that Akkermansia regulates disease
209 through innate, adjuvant-like mechanisms that shape the T-cell effector response
210 phenotype, as well as indirectly by modulating SCFA-producing Firmicutes. This working
211 model is depicted in Figure 6a.

212 **6. The inverse relationship between Verrucomicrobia and Firmicutes extends to**
213 **clinical uveitis, multiple sclerosis and Crohn's disease**

214 Because effector Th1 skewing in the Akk-rich gut environment was independent of
215 antigenic specificity, we hypothesized that it could be associated with human
216 inflammatory conditions, such as uveitis, multiple sclerosis (MS) and inflammatory bowel
217 disease (IBD). To establish a common metric for comparing healthy to diseased state, we
218 used the phylum-level ratio of Verrucomicrobia / Firmicutes (V/F ratio) which consistently
219 tracked with disease severity in HuFI mice (Fig. 6b-c). Application of this metric to the
220 entire cohort of our clinical uveitis samples (so as to minimize any selection bias),
221 revealed higher V/F ratios in uveitis patients compared to healthy subjects (Fig. 6d). We
222 next examined publicly available MS[25] and IBD[26] datasets, the latter comprising patients
223 with Crohn's disease and ulcerative colitis (UC). Compared to healthy controls, the V/F
224 ratio in MS, and in Crohn's disease patients—a condition predominantly driven by Th1-
225 mediated inflammation—but not in UC patients[27,28], was markedly elevated (Fig. 6e-f).
226 Taken together, the gut microbial interaction networks indicated a negative correlation of
227 Verrucomicrobia (Akkermansia) with Firmicutes not only in R161H mice, but also in
228 uveitis, MS and Crohn's disease patients, supporting the generality of this relationship.

229

230 **DISCUSSION**

231 In this study, we report a gut microbial interaction network that regulates autoimmune and
232 inflammatory processes along the "gut–eye axis". By integrating data-driven analyses
233 and *in vivo* microbial perturbation, we provide compelling evidence for a negative
234 relationship between Akkermansia and Firmicutes and link it to disease severity.
235 Specifically, Akkermansia appears to promote sEAU in HuFl R161H mice by
236 outcompeting SCFA-producing Firmicutes in the gut, resulting in diminished SCFA levels
237 and enhanced Th1 responses both locally and systemically (Fig. 6a). Our findings
238 provide a mechanistic basis for how the gut microbiome controls ocular autoimmunity,
239 dissect the complex interacting stimuli that underpin this process, and highlight its broadly
240 generalizable nature.

241 Our network-based perspective contrasts with previous studies, which have mostly
242 focused on how individual gut microbial taxa influence disease and host immunity[4].
243 *A. muciniphila* has been implicated across a spectrum of inflammatory and autoimmune
244 diseases[29]. However, different reports have described conflicting functional effects. As an
245 example, Akkermansia has been reported to promote Th1 polarization of human
246 PBMCs[30], and its relative abundance correlated with disease activity in MS patients[25,30-
247 32]. In contrast, in vivo Th1-polarizing activity has not been observed in Akk-
248 monocolonized mice[30] and T cell responses to Akkermansia in SPF mice have not
249 correlated with a consistent T cell effector phenotype[33]. These observations, together
250 with our finding that Akkermansia affects sEAU through interactions that modulate the
251 broader microbial network, support the notion that the immunological impact of
252 Akkermansia—and of any single microbes in general—depends heavily on microbial
253 community context and host factors.

254 The R161H sEAU model provides a platform to dissect these contextual effects. When
255 the model was first established, we identified signaling by a (microbiota-dependent)
256 mimic antigen in the SPF flora of R161H mice as an important, but possibly not the only,
257 disease trigger[2]. In the "humanized" sEAU mice, Akkermansia does not appear to act as
258 a surrogate antigen, suggesting that other HuFl members may provide this function.
259 However, we did not attempt to identify the HuFl microbial mimic, as identifying it would

260 lack translational relevance. The R161 TCR recognizes a mouse class II (I-A^r)-restricted
261 epitope of IRBP. Human MHC class II molecules would almost certainly present a
262 different epitope(s) from any given antigen than does mouse I-A^r, plus the epitope(s)
263 would differ between individuals, given the heterogeneity of human MHC haplotypes.
264 Moreover, whereas IRBP is a dominant retinal autoantigen in mice, human uveitis more
265 commonly involves recall responses to arrestin[1]. Therefore, although the HuFl R161H
266 sEAU model cannot reveal specific antigenic targets involved in human uveitis, it can
267 reveal conserved mechanisms shared across species, such as the microbial interaction
268 network identified in this study.

269 A key feature of this microbial network is the negative relationship between Akkermansia
270 and Firmicutes, which links gut microbial composition to systemic inflammation. This
271 antagonism likely arises from multiple, non-mutually exclusive mechanisms. Both taxa
272 are dominant colonizers of the colon and may engage in direct niche competition and
273 indirect interactions. Akkermansia promotes mucus degradation during gut
274 inflammation[34,35]. The compromised mucus barrier would exacerbate inflammation and
275 oxidative stress[36], creating inhospitable conditions for obligate anaerobes like Firmicutes.
276 Finally, while Akk antagonizes SCFA-producing Firmicutes, their SCFAs can in turn act to
277 suppress Akkermansia growth and mucolytic activity[37].

278 All those interactions are reflected in the V/F ratio, which may serve as an indicator of
279 inflammatory state and immune polarization across species, supporting its translational
280 value. A similar “legacy” metric Firmicutes to Bacteroidetes (F/B ratio) has been used to
281 indicate overall shifts in gut microbiome composition, but is now being phased out due to
282 its inconsistent disease associations[38,39]. We propose that the V/F ratio is more
283 specifically informative in autoimmune and inflammatory settings.

284 Of note, numerous studies report an association between uveitic diseases and gut
285 inflammation. Uveitis is associated with an increased risk of Crohn’s (but not of UC)[40],
286 and Crohn’s patients are more likely than UC patients to develop uveitis[41]. The findings
287 are compatible with the notion that the V/F ratio increases under conditions where gut
288 inflammation co-occurs with extraintestinal autoimmunity. The V/F ratio may also rise

289 under Th1-dominant inflammatory conditions, as observed in our data. Our analyses
290 reveal elevated V/F ratios not only in our patients with uveitis, but also in published
291 datasets from patients with MS[25] and IBD[26]. Within IBD, increases in V/F were evident in
292 Crohn's disease (Th1-dominant[42-44]), but not in UC (Th2-like[45-47]).

293 Limitations of the study: The complexity of the Akkermansia–Firmicutes axis poses a
294 major challenge to resolving microbial relationships at species and strain levels.
295 Emerging approaches such as bacterial spatial transcriptomics[48] are not yet sufficiently
296 developed to define the precise mechanisms by which Akkermansia antagonizes SCFA-
297 producing Firmicutes. In addition, the finite capacity of our GF R161H colony constrains
298 the scale and breadth of gnotobiotic experiments. Consequently, several mechanistic
299 studies, including administering individual SCFAs to HuFl mice for functional validation,
300 could not be completed within a feasible time frame.

301 In conclusion, our findings show that a complex microbial interaction network—rather
302 than individual taxa—plays a central role in shaping the gut–eye axis. The Akkermansia–
303 Firmicutes relationship likely represents a generalizable ecological principle in which
304 microbial competition influences systemic immune balance and susceptibility to
305 autoimmunity and inflammation, and which extends across species. Future studies aimed
306 at defining the mechanisms by which Akkermansia gains an advantage over SCFA-
307 producing Firmicutes, may guide the development of microbiome-based interventions for
308 autoimmune and inflammatory diseases that intersect with gut dysregulation.
309

310 **METHODS**

311 ***Mice.*** R161H mice on the B10.RIII background[10] were bred in-house and maintained
312 under SPF conditions and fed standard facility chow *ad libitum*. GF and HuFl R161H
313 mice were maintained in the gnotobiotic isolators. The animal study protocol (NEI-688)
314 was approved by the NEI Institutional Animal Care and Use Committee.

315 ***Generation of gnotobiotic mice with human stool samples.*** Human stool samples of
316 healthy volunteers were collected at Keio University according to the study protocol[49]
317 approved by the Institutional Review Boards (approval number 20150075) and informed
318 consent was obtained from each subject. Stool samples were suspended in 20% glycerol
319 in PBS, snap frozen in liquid nitrogen and stored at -80°C. The U, V, and W stocks were
320 thawed and gavaged into GF R161H mice and individual cohort lines were established in
321 separate germ-free isolators.

322 ***Evaluation of uveitis phenotype.*** Development of uveitis was monitored by fundoscopic
323 observation via a binocular microscope of anesthetized mice at the indicated age. For
324 histopathology, eyes were enucleated and fixed in 4% glutaraldehyde for 1 h and
325 transferred to 10% formaldehyde for additional 24 h, embedded in methacrylate, and
326 processed for H&E staining. Disease scores of fundoscopy and histology were assigned
327 by a masked observer on a scale of 0–4, according to the criteria for EAU scoring
328 described in detail elsewhere which are based on the number, size and type of lesions[50].

329 ***HuFl R161H fecal suspension preparation.*** Cecal and colonic contents from HuFl mice
330 of varying disease severity were collected under sterile conditions and immediately
331 transferred on ice to an anaerobic chamber (Coy Laboratory Products). Contents were
332 filtered three times through a 70 μm cell strainer in 20% glycerol–PBS, and aliquoted to
333 prevent repeated freeze–thaw cycles. Each sample was prepared from either individual
334 mice or pools of mice with the same disease severity. The baseline HuFl suspension for
335 reconstitution experiments was prepared from two mice with low uveitis scores and
336 validated by 16S sequencing to contain ~1% Akkermansia (ranges 1–8% in tested
337 samples).

338 ***In vivo microbial enrichment by gnotobiotic reconstitution.*** *A. muciniphila* or *E. coli*
339 were cultured in mucin-BHI media inside the anaerobic chamber or in LB media in the
340 aerobic incubator, respectively. Microbial monoculture was prepared in advance and the
341 first passage timed to reach the exponential growth phase immediately prior to oral
342 gavage. On the day of gavage, GF R161H were transferred from the gnotobiotic isolators
343 to sterile and static microisolator cages with a Reemay filter top. Using sterile techniques,
344 these mice were examined by fundoscopy and assigned to experimental or control
345 groups based on initial uveitis disease scores, age and sex. While mice were recovering
346 from anesthesia, gavage material was prepared inside the anaerobic chamber for *A.*
347 *muciniphila* or in the aerobic bacterial hood for *E. coli*, or sterile PBS, which in the "HuFI
348 base model" was combined with the selected HuFI fecal suspension, so each mouse in
349 the experimental group would receive an additional ~10^8 CFU of the microbe of interest in
350 200uL HuFI fecal suspension via oral gavage. Fecal sampling and fundoscopy scoring
351 were performed on a weekly basis, and mice were handled under sterile protocols, with
352 cages opened only inside a biosafety cabinet.

353 ***Fecal DNA extraction and quantification of microbes.*** Fecal pellets were collected
354 from individual mice, immediately frozen on dry ice and stored at -80°C until bacterial
355 DNA extraction in house as previously described[51] or by the NCI Genetics and
356 Microbiome Core. Absolute abundance of bacteria in each fecal sample was assessed by
357 quantitative polymerase chain reaction (qPCR) using Akkermansia or *E. coli* standard
358 curves with Fast SYBR Green Supermix (Applied Biosystems, Waltham, MA, USA) and
359 run on a QuantStudio™ 7 Pro Real-Time PCR System (Applied Biosystems). Specific
360 primers for Akkermansia were Akk.mu3.Fwd (5'-
361 GCGTAGGCTGTTTCGTAAGTCGTGTGTGAAAG -3') and Akk.mu3.Rvs (5'-
362 GAGTGTTCCCGATATCTACGCATTTCA -3')[52], and for *E. coli* were Uni515F (5'-
363 GTGCCAGCMGCCGCGGTAA -3') and Ent826R (5'-
364 GCCTCAAGGGCACAACCTCCAAG -3')[53]. Five ng of fecal DNA was amplified per 10 µL
365 reaction with the following cycling conditions: initial denaturation at 95 °C for 20 sec,
366 followed by 40 cycles of 95 °C for 3 sec and 63 °C for 30 sec. A melt-curve analysis was
367 included at the end of each run to confirm amplification specificity. Bacterial counts (CFU)

368 per 5 ng of DNA were extrapolated from fitted standard curves correlating Cq values with
369 bacterial quantity.

370 ***16S rRNA gene sequencing and analyses.*** Fecal samples were processed at the NCI
371 Genetics and Microbiome Core for 16S rRNA gene sequencing as detailed in prior
372 work[51]. 16S amplicon sequence variants (ASV) were inferred with YAMS16 v1.7
373 (https://github.com/jhbadger/YAMS16), a pipeline running DADA2[54], and taxonomically
374 classified using the SILVA reference database (release 138.1)[55]. Microbial diversity,
375 differential abundance and multivariable association analyses were performed with
376 phyloseq v1.42.0[56], MaAsLin2 v1.12.0[57], microViz v0.12.3[58], and custom scripts in R.
377 Microbial association networks were analyzed with NetCoMi[59]. (NCBI SRA submission in
378 progress)

379 ***Shotgun metagenomic sequencing and analyses.*** Selected DNA samples were
380 submitted to CosmosID, Inc. (Germantown, MD, USA) for shallow shotgun sequencing (3
381 million reads per sample). Specifically, DNA libraries were prepared using the Nextera XT
382 DNA Library Preparation Kit (Illumina, Inc., San Diego, CA, USA) and IDT Unique Dual
383 Indexes with total DNA input of 1 ng. Genomic DNA was fragmented using a proportional
384 amount of Illumina Nextera XT fragmentation enzyme. Unique dual indexes were added
385 to each sample followed by 12 cycles of PCR to construct libraries. DNA libraries were
386 purified using AMpure magnetic Beads (Beckman Coulter, Inc., Brea, CA, USA) and
387 eluted in QIAGEN EB buffer. DNA libraries were quantified using Qubit 4 fluorometer and
388 Qubit™ dsDNA HS Assay Kit. Libraries were then sequenced on the Element AVITI
389 platform 2x150 bp. JAMS v1.9.9[60] and HUMAnN v3.9[61] were used for taxonomic and
390 functional profiling, and genes involved in metabolic pathways of the main SCFAs
391 (acetate, butyrate and propionate) were identified based on InterPro, Gene Ontology and
392 Pfam annotations, and those present in the uveitis datasets were compared between
393 diseased and healthy groups. (NCBI SRA submission in progress)

394 ***Targeted metabolomics and cytokine quantification.*** Cecal and colonic contents
395 (collectively referred to as “fecal contents”), eyes, and serum were collected from age-
396 matched mice at harvest. Eyes were fixed for histological analysis as described above.

397 Fecal and serum samples were snap-frozen on dry ice and stored at −80 °C. For
398 metabolite profiling, at least 100 mg of fecal contents and 150 µL of serum per mouse
399 were transferred to designated tubes and shipped on dry ice to Metabolon, Inc.
400 (Morrisville, NC, USA) for absolute quantification of eight short-chain fatty acids (acetic,
401 propionic, butyric, isobutyric, 2-methylbutyric, valeric, isovaleric, and hexanoic acids).
402 Serum cytokine concentrations were measured using the Mouse Inflammation Panel (13-
403 plex, LEGENDplex™, BioLegend, San Diego, CA, USA) according to the manufacturer's
404 instructions. Data were acquired on a CytoFlex LX flow cytometer (Beckman coulter) and
405 analyzed with LEGENDplex Data Analysis Software (BioLegend) to quantify cytokine
406 levels based on standard curves.

407 ***Tissue harvesting and flow cytometry analyses.*** Peripheral lymphoid tissues
408 (submandibular lymph nodes, spleen, peripheral lymph nodes, mesenteric lymph nodes),
409 and gut lamina propria from small intestine and colon were collected and prepared for
410 single cell suspensions as described elsewhere[2]. Cells were stained with fluorochrome-
411 conjugated antibodies from BD Biosciences, BioLegend or Thermo Fisher Scientific, and
412 viability dyes from Beckman Coulter. Fluorescence-activated cell sorting analyses were
413 done using CytoFlex LX (Beckman coulter). FlowJo v10 (BD Biosciences) was used for
414 data analyses.

415 ***In vitro activation assay on retina-specific T cells.*** IRBP-specific T cells were
416 harvested from spleen and peripheral lymph nodes of *Tcra*$^{-/-}$ *Nr4a1*^{EGFP} (Nur77^{GFP})
417 R161H mice and were enriched for naïve CD4^{+} cells by negative selection (EasySep,
418 StemCell Technologies). CD11c^{+} dendritic cells were purified from spleen WT B10.RIII
419 mice (Miltenyi Biotec) as antigen-presenting cells. T cells and dendritic cells were co-
420 cultured at a 4:1 ratio in the presence of heat-killed *A. muciniphila*, heat-killed *E. coli*, or
421 bacteria-rich extracts. T cell activation was assessed after 22 h by flow cytometric
422 analysis of CD69 and Nur77 expression.

423 ***5' single cell RNAseq sample processing.*** Colon LP cells were labeled with anti-
424 mouse TotalSeqC-HashTags and cell surface antibodies, and sorted for live CD45^{+} and
425 CD4^{+} populations using FACSAria III/Fusion sorters (BD Biosciences). Post-sort viability

426 exceeded 80%, and hash-tagged samples were pooled at equal ratios within each
427 experimental group, combining $CD45^+$ and $CD4^+$ fractions at 1:1 ratio to enrich for $CD4^+$
428 T cells. Pooled cells were resuspended in PBS with 0.04% BSA and loaded onto a 10x
429 Genomics Chromium X instrument at 700–1200 cells/μL for single cell 5' gene expression
430 and TCR profiling. Libraries were prepared using the Chromium Next GEM Single Cell 5'
431 Reagent Kits v2 (Dual Index) following the manufacturer's protocol, and sequenced on
432 NovaSeq 6000 platform (Illumina, Inc., San Diego, CA, USA).

433 ***Single cell RNAseq data analyses.*** Sequencing data were processed with Cell Ranger
434 v9.0.1 (10x Genomics) for demultiplexing and alignment to the Mus musculus reference
435 (GRCm39, Genome Reference Consortium, 2024). Cell doublets were detected and
436 removed using Scrublet v0.2.3[62]. Cells exhibiting high mitochondrial transcript content (≥
437 5%) or abnormal gene counts (< 500 or > 8000) were excluded. Expression data were
438 log-normalized and scaled using the Scanpy v1.11.0[63] in Python v3.10. Dimensionality
439 reduction was performed using Principal Component Analysis (PCA) followed by Uniform
440 Manifold Approximation and Projection (UMAP), and cell clusters were identified with the
441 Leiden algorithm[64]. Cell type annotation was based on computational classification using
442 SingleR v2.8.0[65] with mouse immune reference data from celldex::ImmGenData v1.16.0
443 in R v4.4, as well as the expression of canonical cell type marker genes, and validated by
444 cell lineage–specific surface antibody. The expression of both Trav16 and Trbv5 in a CD4
445 T cell was the standard used to identify IRBP-specific T cells[10]. (NCBI SRA and GEO
446 submission in progress)

447 ***NEI clinical samples and public human data.*** Stool samples were obtained from
448 patients with autoimmune uveitis and healthy controls enrolled in a clinical cohort at the
449 National Eye Institute (NEI), National Institutes of Health (NIH). All participants provided
450 written informed consent under the protocol approved by the Institutional Review Board
451 (Protocol 13-EI-0072). A stratified cohort of treatment-naïve autoimmune uveitis was
452 selected for in-depth gut microbial network analysis, representing primarily posterior- and
453 pan-uveitis cases and ocular-restricted phenotypes such as idiopathic uveitis and
454 birdshot chorioretinopathy. 16S rRNA gene and shotgun metagenomic sequencing of
455 human fecal samples were performed by the Microbiome Cores at the NCI and the

456 Goodman-Luskin Microbiome Center (Los Angeles, CA, USA). Public microbiome data of
457 IBD patients' stool are from PRJNA1198911[26], and that of MS patient stool from the
458 International MS Microbiome Study (iMSMS)[25].

459 ***Statistical analyses.*** Statistical analyses were conducted with R v4.4, Python v3.10, and
460 GraphPad Prism v10.5.0. Non-parametric tests such as Mann-Whitney U and Kruskal-
461 Wallis tests were used for most comparisons between two or more groups. Group
462 differences in multivariate community structure were evaluated by Permutational
463 Multivariate Analysis of Variance (PERMANOVA). Pearson's or Spearman's rank
464 correlation, as well as multivariable association (MaAsLin2 and equivalent methods) were
465 used to assess associations between microbial features and disease or immune
466 phenotypes. P-values were adjusted for multiple comparisons using the false discovery
467 rate (FDR) where applicable, and statistical significance was indicated as follows: * $P < 0.05$, ** $P < 0.01$, *** $P < 0.001$, and **** $P < 0.0001$. Data in bar plots are presented as
468
469 mean values ± SEMs.

470 **REFERENCES**

471 1 Caspi, R. R. A look at autoimmunity and inflammation in the eye. *J Clin Invest* **120**, 3073-
472 3083 (2010).
473 2 Horai, R. *et al.* Microbiota-Dependent Activation of an Autoreactive T Cell Receptor
474 Provokes Autoimmunity in an Immunologically Privileged Site. *Immunity* **43**, 343-353
475 (2015).
476 3 Horai, R. & Caspi, R. R. Microbiome and Autoimmune Uveitis. *Front Immunol* **10**, 232
477 (2019).
478 4 Salvador, R., Zhang, A., Horai, R. & Caspi, R. R. Microbiota as Drivers and as Therapeutic
479 Targets in Ocular and Tissue Specific Autoimmunity. *Front Cell Dev Biol* **8**, 606751 (2020).
480 5 White, Z. *et al.* Gut inflammation promotes microbiota-specific CD4 T cell-mediated
481 neuroinflammation. *Nature* **643**, 509-518 (2025).
482 6 Lee, H. G. *et al.* Pathogenic function of bystander-activated memory-like CD4(+) T cells in
483 autoimmune encephalomyelitis. *Nat Commun* **10**, 709 (2019).
484 7 Miller, S. D. *et al.* Persistent infection with Theiler's virus leads to CNS autoimmunity via
485 epitope spreading. *Nat Med* **3**, 1133-1136 (1997).
486 8 Deeg, C. A., Amann, B., Raith, A. J. & Kaspers, B. Inter- and intramolecular epitope
487 spreading in equine recurrent uveitis. *Invest Ophthalmol Vis Sci* **47**, 652-656 (2006).
488 9 Ji, Q., Perchellet, A. & Goverman, J. M. Viral infection triggers central nervous system
489 autoimmunity via activation of CD8+ T cells expressing dual TCRs. *Nat Immunol* **11**, 628-
490 634 (2010).

491 10 Horai, R. *et al.* Breakdown of immune privilege and spontaneous autoimmunity in mice
492 expressing a transgenic T cell receptor specific for a retinal autoantigen. *J Autoimmun* **44**,
493 21-33 (2013).
494 11 Nakamura, Y. K. *et al.* Gut Microbial Alterations Associated With Protection From
495 Autoimmune Uveitis. *Invest Ophthalmol Vis Sci* **57**, 3747-3758 (2016).
496 12 Shimizu, J. *et al.* Bifidobacteria Abundance-Featured Gut Microbiota Compositional
497 Change in Patients with Behcet's Disease. *PLoS One* **11**, e0153746 (2016).
498 13 Huang, X. *et al.* Gut Microbiota Composition and Fecal Metabolic Phenotype in Patients
499 With Acute Anterior Uveitis. *Invest Ophthalmol Vis Sci* **59**, 1523-1531 (2018).
500 14 Kalyana Chakravarthy, S. *et al.* Dysbiosis in the Gut Bacterial Microbiome of Patients with
501 Uveitis, an Inflammatory Disease of the Eye. *Indian J Microbiol* **58**, 457-469 (2018).
502 15 Ye, Z. *et al.* A metagenomic study of the gut microbiome in Behcet's disease. *Microbiome*
503 **6**, 135 (2018).
504 16 Ye, Z. *et al.* Altered gut microbiome composition in patients with Vogt-Koyanagi-Harada
505 disease. *Gut Microbes* **11**, 539-555 (2020).
506 17 Steimle, A. *et al.* Gut microbial factors predict disease severity in a mouse model of
507 multiple sclerosis. *Nat Microbiol* **9**, 2244-2261 (2024).
508 18 Luger, D. *et al.* Either a Th17 or a Th1 effector response can drive autoimmunity:
509 conditions of disease induction affect dominant effector category. *J Exp Med* **205**, 799-
510 810 (2008).
511 19 Damsker, J. M., Hansen, A. M. & Caspi, R. R. Th1 and Th17 cells: adversaries and
512 collaborators. *Ann N Y Acad Sci* **1183**, 211-221 (2010).
513 20 Horai, R. & Caspi, R. R. Cytokines in autoimmune uveitis. *J Interferon Cytokine Res* **31**, 733-
514 744 (2011).
515 21 Mann, E. R., Lam, Y. K. & Uhlig, H. H. Short-chain fatty acids: linking diet, the microbiome
516 and immunity. *Nat Rev Immunol* **24**, 577-595 (2024).
517 22 Nakamura, Y. K. *et al.* Short chain fatty acids ameliorate immune-mediated uveitis
518 partially by altering migration of lymphocytes from the intestine. *Sci Rep* **7**, 11745 (2017).
519 23 Chen, X. *et al.* Sodium butyrate regulates Th17/Treg cell balance to ameliorate uveitis via
520 the Nrf2/HO-1 pathway. *Biochem Pharmacol* **142**, 111-119 (2017).
521 24 Louis, P. & Flint, H. J. Formation of propionate and butyrate by the human colonic
522 microbiota. *Environ Microbiol* **19**, 29-41 (2017).
523 25 iMSMS Consortium. Gut microbiome of multiple sclerosis patients and paired household
524 healthy controls reveal associations with disease risk and course. *Cell* **185**, 3467-3486
525 e3416 (2022).
526 26 Orejudo, M. *et al.* Exploration of fecal microbiota in newly diagnosed patients with
527 inflammatory bowel disease using shotgun metagenomics. *Front Cell Infect Microbiol* **15**,
528 1595884 (2025).
529 27 Strober, W., Fuss, I. & Mannon, P. The fundamental basis of inflammatory bowel disease.
530 *J Clin Invest* **117**, 514-521 (2007).
531 28 Guan, Q. A Comprehensive Review and Update on the Pathogenesis of Inflammatory
532 Bowel Disease. *J Immunol Res* **2019**, 7247238 (2019).

533 29 Cani, P. D., Depommier, C., Derrien, M., Everard, A. & de Vos, W. M. Akkermansia
534 muciniphila: paradigm for next-generation beneficial microorganisms. *Nat Rev*
535 *Gastroenterol Hepatol* **19**, 625-637 (2022).
536 30 Cekanaviciute, E. *et al.* Gut bacteria from multiple sclerosis patients modulate human T
537 cells and exacerbate symptoms in mouse models. *Proc Natl Acad Sci U S A* **114**, 10713-
538 10718 (2017).
539 31 Berer, K. *et al.* Gut microbiota from multiple sclerosis patients enables spontaneous
540 autoimmune encephalomyelitis in mice. *Proc Natl Acad Sci U S A* **114**, 10719-10724
541 (2017).
542 32 Jangi, S. *et al.* Alterations of the human gut microbiome in multiple sclerosis. *Nat*
543 *Commun* **7**, 12015 (2016).
544 33 Ansaldo, E. *et al.* Akkermansia muciniphila induces intestinal adaptive immune responses
545 during homeostasis. *Science* **364**, 1179-1184 (2019).
546 34 Desai, M. S. *et al.* A Dietary Fiber-Deprived Gut Microbiota Degrades the Colonic Mucus
547 Barrier and Enhances Pathogen Susceptibility. *Cell* **167**, 1339-1353 e1321 (2016).
548 35 Tingler, A. M. & Engevik, M. A. Breaking down barriers: is intestinal mucus degradation by
549 Akkermansia muciniphila beneficial or harmful? *Infect Immun* **93**, e0050324 (2025).
550 36 Sugihara, K. *et al.* Mucolytic bacteria license pathobionts to acquire host-derived
551 nutrients during dietary nutrient restriction. *Cell Rep* **40**, 111093 (2022).
552 37 Schwabkey, Z. I. *et al.* Diet-derived metabolites and mucus link the gut microbiome to
553 fever after cytotoxic cancer treatment. *Sci Transl Med* **14**, eabo3445 (2022).
554 38 Magne, F. *et al.* The Firmicutes/Bacteroidetes Ratio: A Relevant Marker of Gut Dysbiosis
555 in Obese Patients? *Nutrients* **12** (2020).
556 39 Walters, W. A., Xu, Z. & Knight, R. Meta-analyses of human gut microbes associated with
557 obesity and IBD. *FEBS Lett* **588**, 4223-4233 (2014).
558 40 Lo, T. C., Chen, Y. Y. & Chen, H. H. Risk of inflammatory bowel disease in uveitis patients: a
559 population-based cohort study. *Eye (Lond)* **36**, 1288-1293 (2022).
560 41 Lin, H. *et al.* Differences in the prevalence of uveitis between Crohn's disease and
561 ulcerative colitis: A systematic review and meta-analysis. *Acta Ophthalmol* **102**, e485-
562 e492 (2024).
563 42 Bouma, G. & Strober, W. The immunological and genetic basis of inflammatory bowel
564 disease. *Nat Rev Immunol* **3**, 521-533 (2003).
565 43 Fuss, I. J. *et al.* Disparate CD4+ lamina propria (LP) lymphokine secretion profiles in
566 inflammatory bowel disease. Crohn's disease LP cells manifest increased secretion of IFN-
567 gamma, whereas ulcerative colitis LP cells manifest increased secretion of IL-5. *J Immunol*
568 **157**, 1261-1270 (1996).
569 44 Parronchi, P. *et al.* Type 1 T-helper cell predominance and interleukin-12 expression in the
570 gut of patients with Crohn's disease. *Am J Pathol* **150**, 823-832 (1997).
571 45 Fuss, I. J. *et al.* Nonclassical CD1d-restricted NK T cells that produce IL-13 characterize an
572 atypical Th2 response in ulcerative colitis. *J Clin Invest* **113**, 1490-1497 (2004).
573 46 Heller, F. *et al.* Interleukin-13 is the key effector Th2 cytokine in ulcerative colitis that
574 affects epithelial tight junctions, apoptosis, and cell restitution. *Gastroenterology* **129**,
575 550-564 (2005).

576 47 Strober, W. & Fuss, I. J. Proinflammatory cytokines in the pathogenesis of inflammatory
577 bowel diseases. *Gastroenterology* **140**, 1756-1767 (2011).
578 48 Sarfatis, A., Wang, Y., Twumasi-Ankrah, N. & Moffitt, J. R. Highly multiplexed spatial
579 transcriptomics in bacteria. *Science* **387**, eadr0932 (2025).
580 49 Tanoue, T. *et al.* A defined commensal consortium elicits CD8 T cells and anti-cancer
581 immunity. *Nature* **565**, 600-605 (2019).
582 50 Horai, R. & Caspi, R. R. in *Animal Models for Retinal Diseases. Neuromethods.* Vol. 46
583 207-225 (SpringerLink, 2010).
584 51 Salvador, R. *et al.* Too Much of a Good Thing: Extended Duration of Gut Microbiota
585 Depletion Reverses Protection From Experimental Autoimmune Uveitis. *Invest*
586 *Ophthalmol Vis Sci* **64**, 43 (2023).
587 52 Goux, H. J., Chavan, D., Crum, M., Kourentzi, K. & Willson, R. C. Akkermansia muciniphila
588 as a Model Case for the Development of an Improved Quantitative RPA Microbiome
589 Assay. *Front Cell Infect Microbiol* **8**, 237 (2018).
590 53 Barman, M. *et al.* Enteric salmonellosis disrupts the microbial ecology of the murine
591 gastrointestinal tract. *Infect Immun* **76**, 907-915 (2008).
592 54 Callahan, B. J. *et al.* DADA2: High-resolution sample inference from Illumina amplicon
593 data. *Nat Methods* **13**, 581-583 (2016).
594 55 Quast, C. *et al.* The SILVA ribosomal RNA gene database project: improved data
595 processing and web-based tools. *Nucleic Acids Res* **41**, D590-596 (2013).
596 56 McMurdie, P. J. & Holmes, S. phyloseq: an R package for reproducible interactive analysis
597 and graphics of microbiome census data. *PLoS One* **8**, e61217 (2013).
598 57 Mallick, H. *et al.* Multivariable association discovery in population-scale meta-omics
599 studies. *PLoS Comput Biol* **17**, e1009442 (2021).
600 58 Barnett, D. J. M., Arts, I. C. W. & Penders, J. microViz: an R package for microbiome data
601 visualization and statistics. *J Open Source Software* **6** 3201 (2021).
602 59 Peschel, S., Muller, C. L., von Mutius, E., Boulesteix, A. L. & Depner, M. NetCoMi: network
603 construction and comparison for microbiome data in R. *Brief Bioinform* **22** (2021).
604 60 McCulloch, J. A. *et al.* JAMS - A framework for the taxonomic and functional exploration
605 of microbiological genomic data. *bioRxiv* (2023).
606 61 Beghini, F. *et al.* Integrating taxonomic, functional, and strain-level profiling of diverse
607 microbial communities with bioBakery 3. *Elife* **10** (2021).
608 62 Wolock, S. L., Lopez, R. & Klein, A. M. Scrublet: Computational Identification of Cell
609 Doublets in Single-Cell Transcriptomic Data. *Cell Syst* **8**, 281-291 e289 (2019).
610 63 Wolf, F. A., Angerer, P. & Theis, F. J. SCANPY: large-scale single-cell gene expression data
611 analysis. *Genome Biol* **19**, 15 (2018).
612 64 Traag, V. A., Waltman, L. & van Eck, N. J. From Louvain to Leiden: guaranteeing well-
613 connected communities. *Sci Rep* **9**, 5233 (2019).
614 65 Aran, D. *et al.* Reference-based analysis of lung single-cell sequencing reveals a
615 transitional profibrotic macrophage. *Nat Immunol* **20**, 163-172 (2019).

616 **Acknowledgments**

617 We are grateful to NEI and NHLBI Flow Cytometry Cores, NEI Histology and Genetic
618 Engineering Cores, Ms. Wuxing Yuan, Dr. Shah Rashed and members of NCI
619 Microbiome Core, UCLA Goodman-Luskin Microbiome Center Microbiome Core, and all
620 members of the Caspi Lab for their invaluable experimental assistance. We extend
621 special thanks to Dr. Katsuko Sudo (Tokyo Medical University, Japan), Mr. Hirofumi
622 Kobayashi and staff at Sankyo Labo Service Corporation, Inc. (Japan), as well as the
623 gnotobiotic management team from NEI Veterinary Research and Resources Section for
624 their expert support and guidance in GF and gnotobiotic colony maintenance. We also
625 thank Dr. Eduard Ansaldo (NIAID) for sharing protocols for Akkermansia culture, Dr.
626 Kikuji Itoh (Japan SLC, Inc.), Dr. Koji Atarashi and members of the Honda Lab for
627 providing experimental advice. Finally, we acknowledge Dr. Geoffrey A. Mueller and staff
628 at NIEHS Nuclear Magnetic Resonance Group for their generous assistance with
629 metabolomics, and Drs. Kelsey Wheeler, Daniel Sellers, and Reuben Allen
630 (Massachusetts Institute of Technology) for their insightful discussions and critical
631 feedback. This study was supported by NIH/NEI Intramural funding, Project Number
632 EY000184.

633 **Author contributions**

634 A.Z., R.H. and R.R.C. conceived and designed the study. R.R.C and R.H. supervised the
635 project. A.Z., R.H., Y.J., A.G., S.A., and C.E.M. performed experiments and collected
636 data. A.Z., J.H.B., Z.W., G.S., and V.N. performed computational analyses. S.H., H.N.S.,
637 J.W.L. and K.H. provided human microbiome samples, and S.K. and H.N.S. contributed
638 to clinical interpretation. X.X., M.J.M., Z.P., B.X. provided experimental input and
639 technical assistance. R.P. and N.M. provided technical expertise in bacteriology. J.H.B.,
640 Z.W., J.A.M., J.P.J. and C.O. contributed analytical tools, resources and expertise. A.Z.
641 and R.H. analyzed and interpreted data and prepared figures. A.Z., R.H. and R.R.C.
642 wrote and finalized the manuscript. All authors discussed the results, reviewed, and
643 approved the final manuscript.

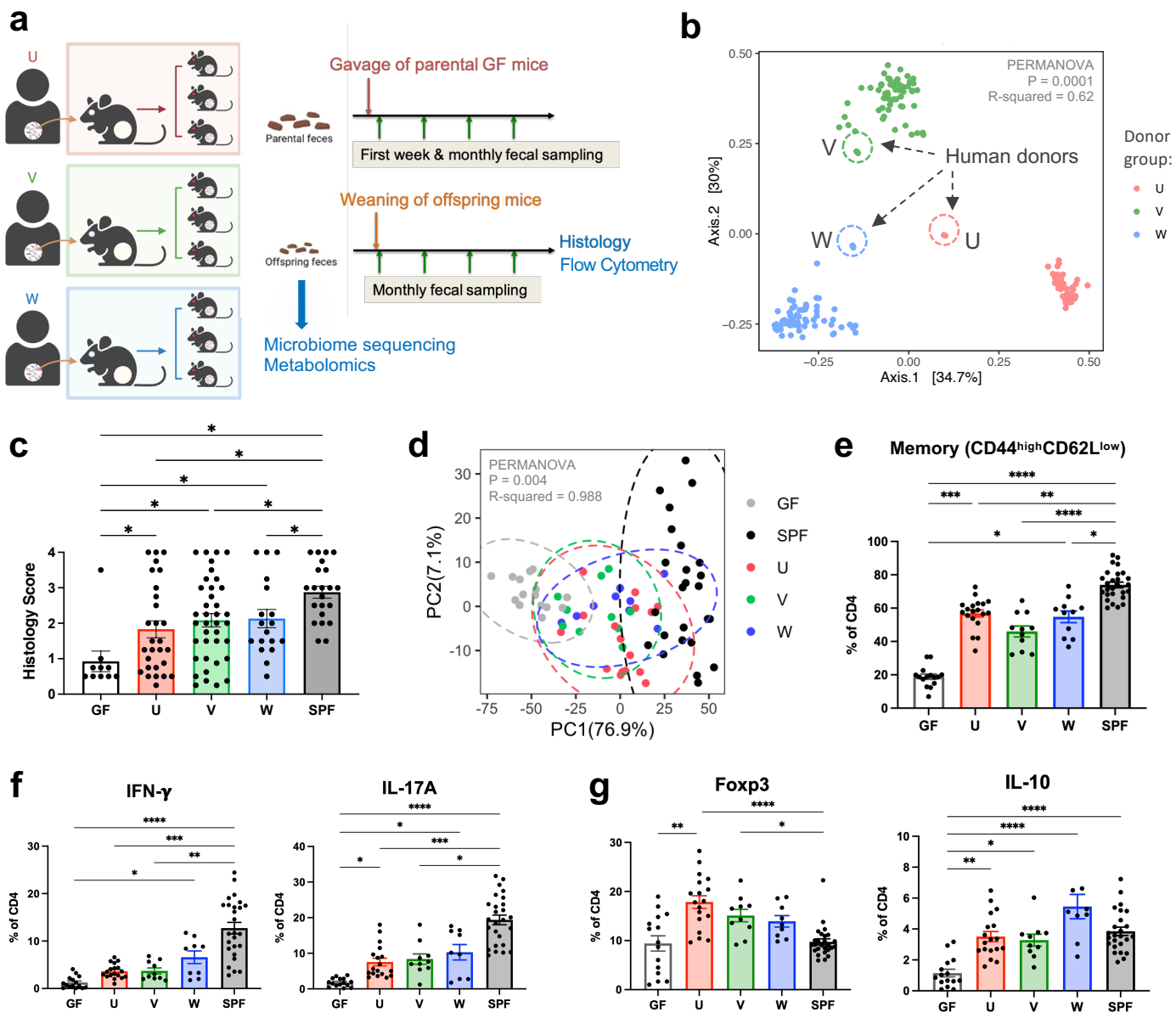

Fig. 1 | Human gut commensals support development of spontaneous experimental autoimmune uveitis (sEAU). a, Schematic representation of human fecal microbiota transfer experiments and data collection. **b**, Beta diversity based on Bray–Curtis dissimilarity showing differences in fecal microbiome composition between recipient groups U (n = 50), V (n = 59), W (n = 64). Encircled with dashed lines are the respective human donor (original) fecal samples. **c**, Disease scores (histology) of age-matched R161H mice (4-5 months old) from human flora (U, V, W, n = 28, 38, 18), SPF (n = 22) and GF (n = 10) groups (Kruskal–Wallis test between mouse recipient groups, p = 0.0002). **d**, Immunological clusters of CD4 T cells from colon lamina propria (LP) by the microbiome groups. PCA analysis performed on immune signature matrix by frequencies of CD4 T cells expressing each cell surface or intracellular marker (see **Extended Data Fig. 1e**). **e**–**g**, Frequencies of memory ($CD44^{high}CD62L^{low}$, **e**), IFN-γ- or IL-17A-producing (**f**), and regulatory (Foxp3-positive or IL-10-producing, **g**) CD4 T cells in colon LP of HuFl, SPF and GF R161H mice. **d**–**g**, Compiled data from 12 experiments, n = 15, 19, 11, 11, 27 for GF, U, V, W and SPF, respectively. Kruskal–Wallis tests show p < 0.0001 (**e**–**g**). P-values adjusted for post hoc multiple comparisons are displayed as asterisks. *P < 0.05, **P < 0.01, ***P < 0.001, ****P < 0.0001, and bar plots showing mean values ± SEMs (**c**, **e**–**g**).

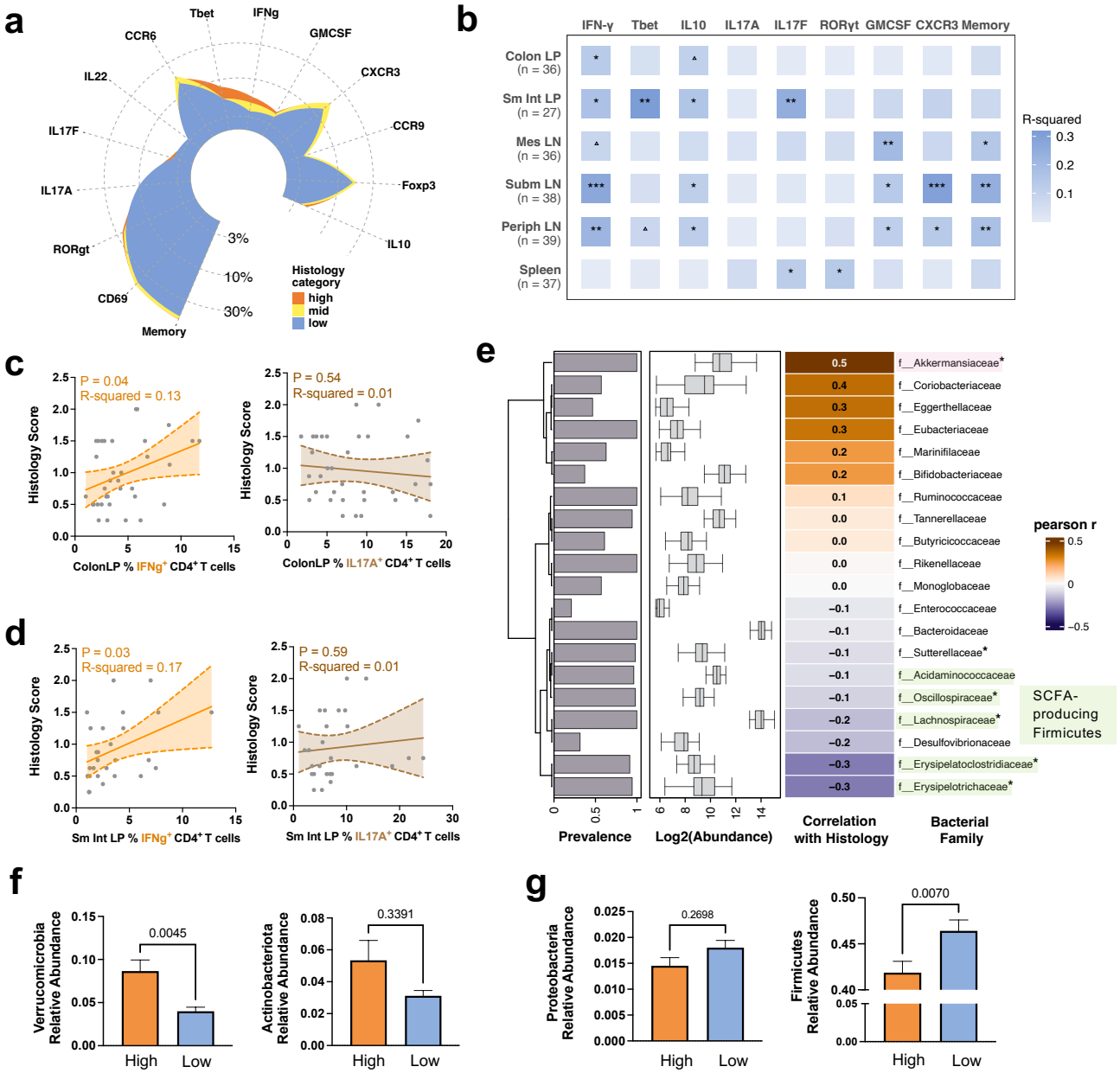

Fig. 2 | HuFl sEAU tracks with a dominant Th1 phenotype and abundance of Verrucomicrobia/Akkermansia. **a**, Mean relative frequency of colon LP CD4 T cells of each cell surface or intracellular marker arranged in a circular plot, colored by histology category: high (score ≥ 1.5, n = 10), mid (0.75 < score < 1.5, n = 8), low (score ≤ 0.75, n = 17). **b**, Correlational heatmap of histology scores with relative frequencies of each cell surface or intracellular marker in CD4 T cells across six tissue sites. LP, lamina propria; LN, lymph nodes; Sm Int, small intestine; Mes, mesenteric; Subm, submandibular; Periph, peripheral. ^0.05 < P < 0.08, *P < 0.05, **P < 0.01, ***P < 0.001, modeled by simple linear regression with R-squared values defining the color gradient. **c**–**d**, Representative trend lines with 95% confidence interval (shaded area) show that disease scores of HuFl mice are positively associated with IFN-γ-producing, but not IL-17A-producing, CD4 T cells, in colon LP (**c**) and small intestine LP (**d**). Data in **a**–**d** are aggregated from 8 experiments (UVW combined, sample sizes ranged from n = 27 to 39 across tissues following quality filtering). **e**, Correlational heatmap showing major fecal bacterial taxa (out of top 20 most abundant families) that correlate with disease scores in adult HuFl R161H (UVW combined, n = 105). P-values assessed after FDR (false discovery rate) correction following Pearson correlation. *P < 0.05. **f**–**g**, More Verrucomicrobia (**f**), and fewer Firmicutes (**g**) are present in the gut of HuFl mice with high disease scores. Sample sizes are n = 36 and 43 for high and low histology categories, respectively. Data in bar plots are presented as mean values ± SEMs, and P-values from Mann-Whitney U tests are shown in plots.

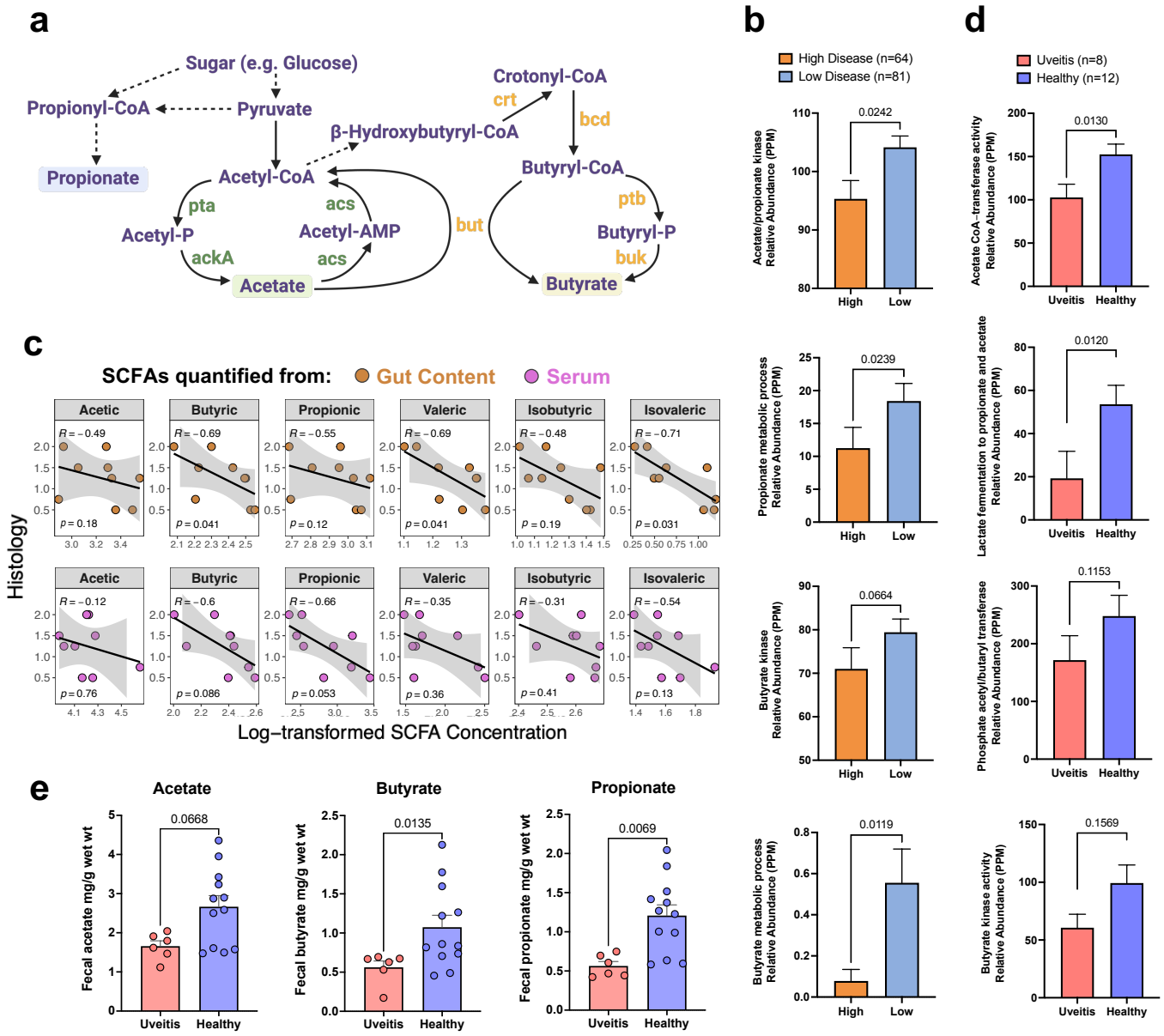

Fig. 3 | SCFA signatures are enriched in low disease HuFl mice or healthy subjects. a, A simplified pathway map highlighting functional genes involved in the main SCFA synthesis and metabolism. Dashed arrows indicate hidden intermediate steps. Abbreviations of enzyme symbols: pta, Phosphotransacetylase; ackA, Acetate kinase; acs, Acetyl-CoA synthetase; but, Butyryl-CoA:acetate CoA-transferase; ptb, Phosphate butyryltransferase; buk, Butyrate kinase; crt, Crotonase; bcd, Butyryl-CoA dehydrogenase. **b**, Enzymes in SCFA pathways (annotated with InterPro and Gene Ontology databases) are enriched in HuFl mouse gut with low histology scores (UVW combined, weanling and adult samples included). PPM, parts per million, a measure of relative abundance based on normalized base count for each feature in a metagenomic sample. **c**, Spearman correlation (visualized with a linear trend line) showing higher disease scores associated with lower SCFA concentrations both locally (in gut content) and systemically (in serum) in representative cohort U mice (n = 9). **d**, Enzymes in SCFA pathways (annotated with Gene Ontology and Pfam databases) are enriched in fecal samples from healthy humans compared to those from treatment-naïve uveitis patients, from a cohort of autoimmune uveitis (ocular-restricted, including idiopathic uveitis, VKH/SO and BCR). Sex, age, race and diet are comparably represented in patient and control groups. Normalized gene abundance is reported in PPM. **e**, SCFA levels from uveitis patients and healthy controls (same cohort as in **d,** but n = 6 available from the patient group). For **b, d** & **e**, Data are presented as mean values ± SEMs. Statistical significance was determined by Mann-Whitney U test.

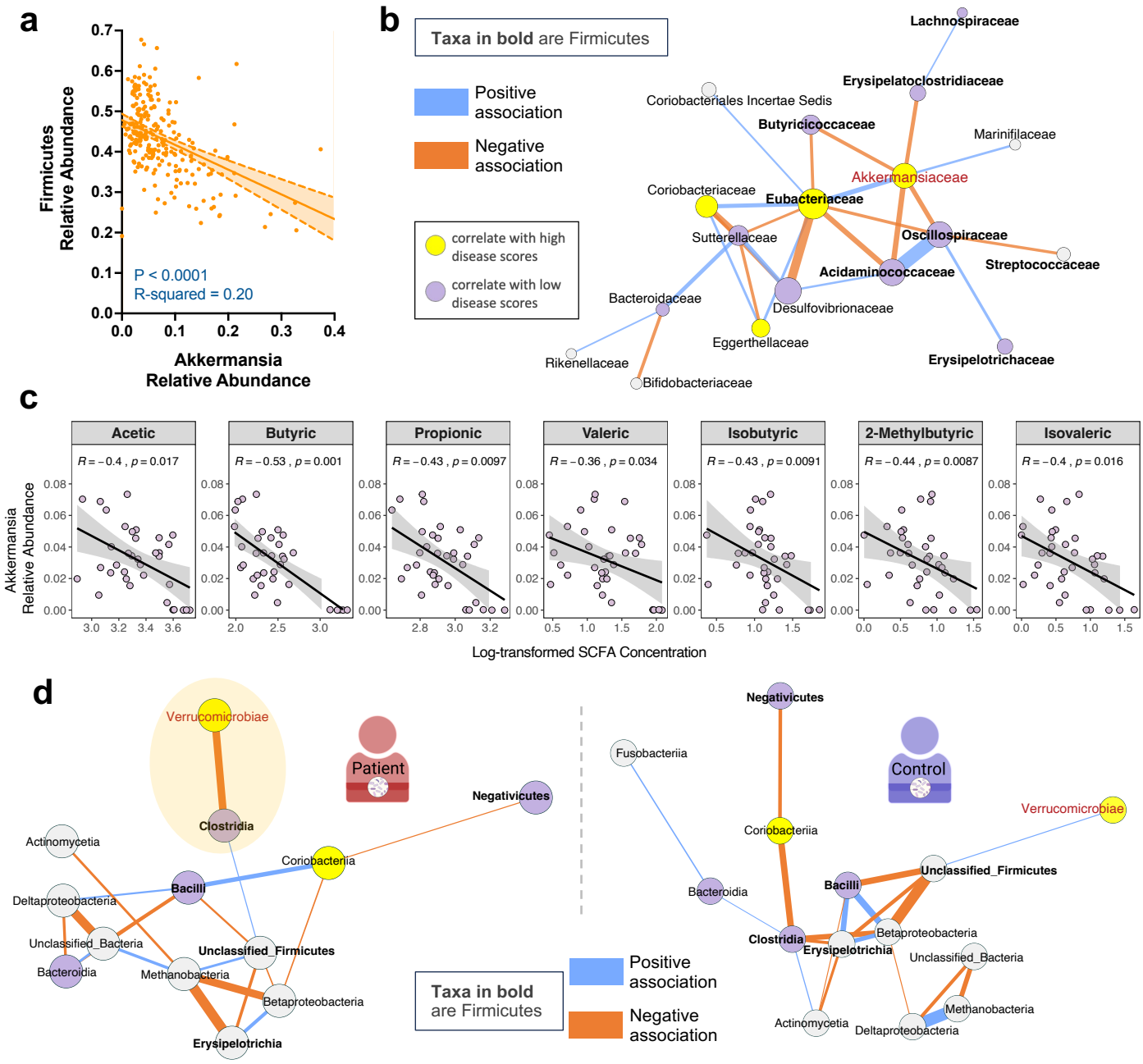

Fig. 4 | Akkermansia negatively correlates with Firmicutes in both sEAU and clinical uveitis. a, Simple linear regression showing a negative correlation of microbial relative abundance between Akkermansia (equivalent to Verrucomicrobia in this dataset) and Firmicutes in HuFl R161H mice (n = 234, UVW combined, weanling and adult samples included). **b**, Fecal bacterial association network exemplified in HuFl cohort V (n = 79, weanling and adult samples included). Network constructed at the taxonomic level of the bacterial family. Correlations with a threshold of Pearson r > 0.5 were transformed into dissimilarities via the "unsigned" distance metric, on which edge weights (strength of correlations) are based. Blue edges correspond to positive associations and orange edges to negative ones. Yellow and purple nodes represent taxa enriched in high *vs.* low disease categories, with Firmicutes labeled as bolded taxon names. Bigger nodes are more influential in the network (higher eigenvector centrality). **c**, Spearman correlation (visualized with a linear trend line) showing a negative association between relative Akkermansia abundance and SCFA concentrations in R161H gut (n = 35, UVW and SPF combined). Akkermansia was selected following multivariable association between SCFA concentrations and microbial features using MaAsLin2. **d**, Class level association networks in treatment-naïve uveitis patients (left, n = 8) and healthy controls (right , n = 12) from the same cohort of autoimmune uveitis. Correlations with a threshold of Pearson r > 0.3 are shown. Node and edge color schemes same as in **b**. Shaded ellipse in the patient network highlights the negative correlation between Verrucomicrobiae (Akkermansia) and Clostridia (Firmicutes), and this relationship is absent from the healthy human gut.

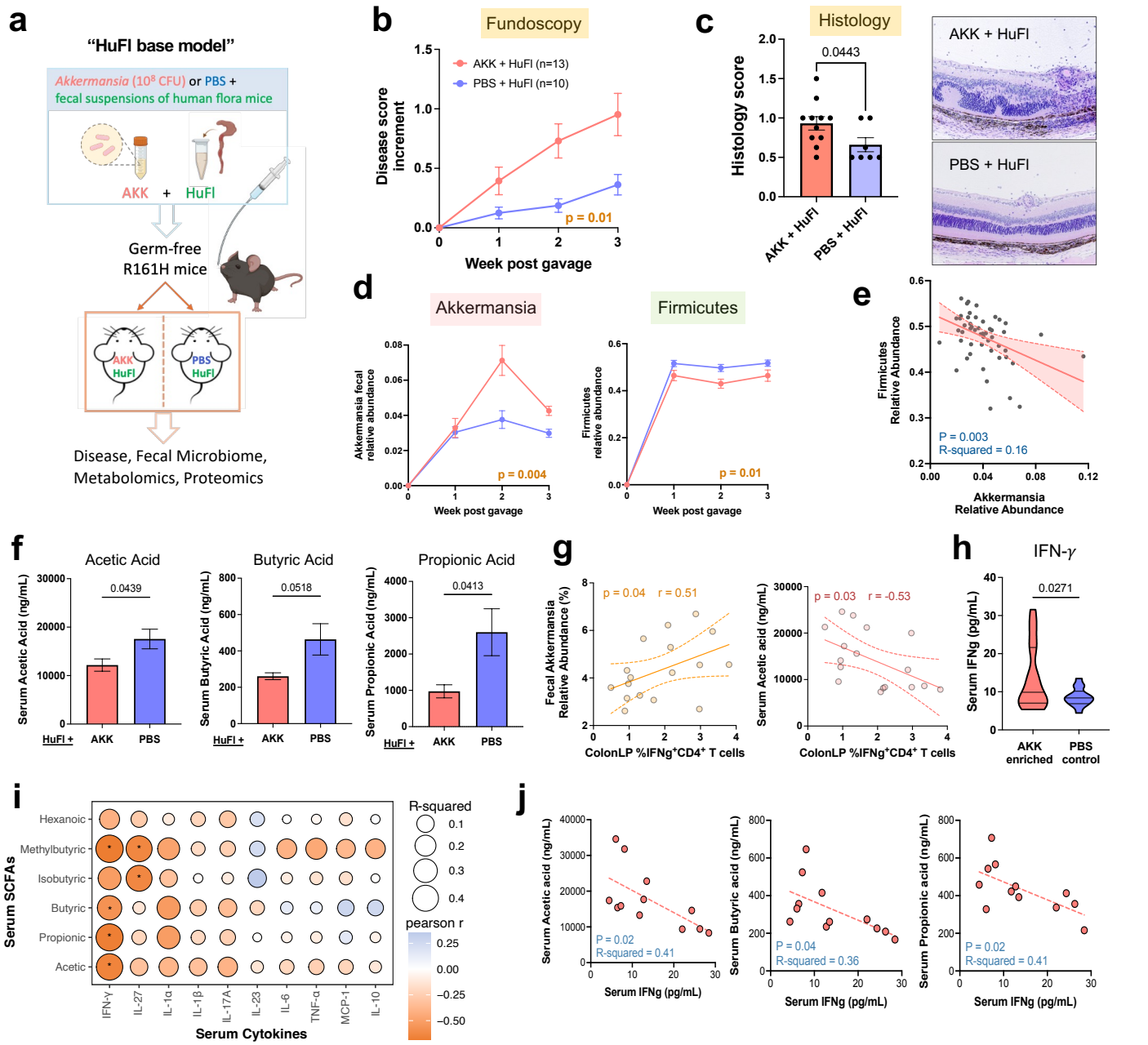

Fig. 5 | Akkermansia promotes uveitis by outcompeting SCFA producers and decreasing circulating SCFA levels. **a**, Study design of microbe reconstitution experiments. **b**, Fundoscopy score increments from starting disease scores of previously GF R161H mice gavaged with a baseline human gut microbiota suspension (HuFl) plus *Akkermansia muciniphila* culture (AKK, 10^8 CFU) or sterile PBS. Data combined from three experiments. **c**, Histology scores and representative images from 2 out of 3 experiments (n = 11 and 7 for Akk-rich and control, respectively). Mean values ± SEM. P-value determined by Welch-corrected t test. **d**, Relative abundance of Akkermansia and Firmicutes in feces from one representative of 3 experiments (n = 7 and 6 for Akk-rich and control, respectively). **e**, A negative correlation of relative abundance between Akkermansia and Firmicutes (n = 52, AKK and PBS groups combined, multiple time points included) by simple linear regression. **f**, Serum concentrations of main SCFAs are significantly lower in Akk-rich (n = 13) mice than in PBS controls (n = 10). Serum harvested 3 – 4 weeks post gavage, three experiments combined. **g**, Spearman correlation (visualized with a linear trend line) showing Akkermansia relative abundance associated positively, and serum acetic acid associated negatively, with the frequency of IFN-γ-producing CD4 T cells in colonic LP. **h**, Akk-enriched (n = 18) mice had higher serum IFN-γ concentrations compared to PBS control mice (n = 14), five experiments combined, of which two experiments used the minimal flora model. **i**, Correlational heatmap of SCFA levels with cytokine concentrations in serum of engrafted mice. *P < 0.05, modeled by simple linear regression as well as Pearson correlation. **j**, Representative trend lines show that main SCFA concentrations are negatively associated with IFN-γ levels in serum. Data in **i**–**j** are from 2 experiments (n = 12) using the minimal flora model.

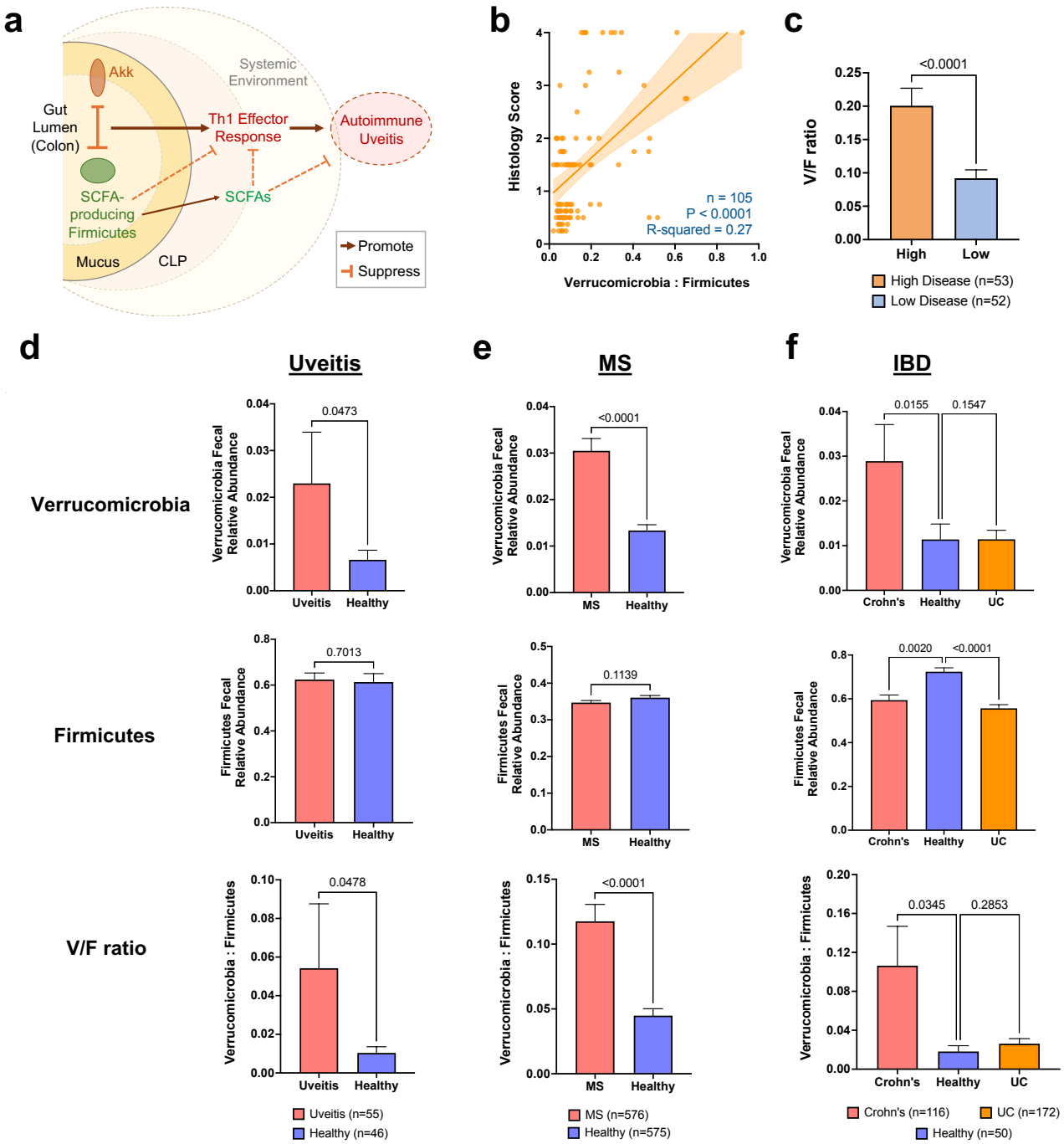

Fig. 6. **The inverse relationship between Verrucomicrobia and Firmicutes extends to clinical uveitis, MS and Crohn's disease. a**, Graphical summary of the working model. Dashed lines are not directly tested. CLP, colon lamina propria. **b**, A positive correlation between Verrucomicrobia/Firmicutes ratios and histology scores of HuFl mice by simple linear regression. **c**, V/F ratio of Verrucomicrobia (Akkermansia) and the Firmicutes phyla compared between high and low disease of HuFl mice as in **b**. **d**, Relative abundance of Verrucomicrobia and Firmicutes, and V/F ratios compared between uveitis patients and healthy controls. Patient cohort included those established on treatment. **e,** Relative abundance of Verrucomicrobia and Firmicutes, and V/F ratios in MS patient cohort and healthy controls, analyzed from public data. **f,** Relative abundance of Verrucomicrobia and Firmicutes, and V/F ratios in IBD (Crohn's disease and UC) patient cohort and healthy controls, analyzed from public data. Data are presented as mean values ± SEM, and statistical significance was determined by Mann-Whitney U test (one-tailed analysis was applied for V/F ratio in **d** & **e**).